

RSC Advances



This is an *Accepted Manuscript*, which has been through the Royal Society of Chemistry peer review process and has been accepted for publication.

Accepted Manuscripts are published online shortly after acceptance, before technical editing, formatting and proof reading. Using this free service, authors can make their results available to the community, in citable form, before we publish the edited article. This *Accepted Manuscript* will be replaced by the edited, formatted and paginated article as soon as this is available.

You can find more information about *Accepted Manuscripts* in the [Information for Authors](#).

Please note that technical editing may introduce minor changes to the text and/or graphics, which may alter content. The journal's standard [Terms & Conditions](#) and the [Ethical guidelines](#) still apply. In no event shall the Royal Society of Chemistry be held responsible for any errors or omissions in this *Accepted Manuscript* or any consequences arising from the use of any information it contains.

Successive *in situ* Synthesis of Ag/PA6 Nanocomposites

Jianping Duan^a, Dajiang Zhao^b, Xingke Zhao^a, Housheng Xia^c, Peng Li^a, Yan liu^c, Guisheng Yang^{a,b,c,*}

A novel approach to *in situ* synthesis of silver/polyamide 6 (Ag/PA6) nanocomposites is reported. The method included two steps: *in situ* preparation of silver nanoparticles (Ag NPs) in molten ϵ -caprolactam (CL), followed by polymerization of residual CL. The CL was used as reducing agent, protecting agent and solvent in the synthesis of Ag NPs, as well as precursor monomers of polyamide 6 in the subsequent polymerization. The formation of Ag NPs was verified by X-ray diffraction. Transmission electron microscopy (TEM) showed that the as-synthesized Ag NPs had a size less than 25 nm and was uniformly embedded in polyamide 6 matrix. Fourier transformed infrared spectrometry (FTIR) and ^{13}C NMR indicated that pre-oxidation of CL had little effect on chemical structure of the polyamide molecules, except for a decrease of molecular weight. The variation in particle size and size distribution of Ag NPs complicated the thermal behaviors of resultant nanocomposites.

1 Introduction

Polycaprolactam or polyamide 6 (PA6), a commercially important polyamide, is derived from ϵ -caprolactam (CL) via hydrolytic or anionic polymerization. Current formulations of PA6 cannot meet the demands of modern society for high performance materials, such as in the fields of engineering or biological materials. The use of PA6 nanocomposites is a promising way to improve the properties related to antibacterial and engineering materials,¹ and many efforts have been devoted to the preparation of PA6 nanocomposites.² The two most convenient routes for preparation of PA6 nanocomposites involve mechanical blending and *in situ* preparation. For mechanical blending, the low viscosity of PA6 in the molten state facilitates the dispersion of nanoparticles.³ Mechanical blending for preparation of PA6 nanocomposite can be divided into two individual steps: preparation/selection of nanoparticles and operation of blending.^{3,4} Properties of resultant PA6 nanocomposites are strongly influenced by the properties of nanoparticles, including size and size distribution. Shearing and heating in the blending operation

determine whether nanoparticles are homogeneously distributed in the PA6 matrix. This eventually influences the resultant properties of nanocomposites. However, nanoparticles used in this method are pre-prepared.^{2,3,5} The characteristics of nanoparticles can seldom be changed in the process of mechanical blending. The concerns in the properties of nanoparticles, such as morphology and/or surface characteristics, cannot be eliminated in either of these two methods.

As a result of the inflexibility inherent in the blending methods, the second preparation method, in which the inorganic phase is grown *in situ*, is being actively pursued globally.⁵ They were prepared by the methods that dispersing nanoparticles in CL molten followed by the polymerization of CL. The nanoparticles used at here were pre-prepared too, analogous to that of mechanical blending. Some representatives of *in situ* preparation of PA6 nanocomposites are solution cast or electrospinning,^{1a,6} in which the solvent of PA6 plays the role of reactant and ensures the generation of nanoparticles, while PA6 acts in the role of protecting agent. These methods were designed for films or fibers. Using extra solvent prevents their use in the large-scale synthesis of bulk PA6 nanocomposites.

The work presented here describes a method for preparation of PA6 nanocomposites by using CL as reagent in the synthesis of nanoparticles, and precursor of polymer matrix in the following polymerization. The CL plays the roles of the reducing agent, protecting agent and solvent in the process of *in situ* generation of silver nanoparticles (Ag NPs). As-synthesized Ag NPs were uniformly distributed in the matrix of PA6 polymerized from residual CL. This successive *in situ* process simplifies the preparation of Ag/PA6 nanocomposites, which may be important for nanofiber and membrane applications.

2 Experimental

2.1 Materials.

Silver nitrate (AgNO_3 , 99.8 wt%) was purchased from Xilong Chemical Co. Ltd. ϵ -caprolactam (CL, 99.5 %) were obtained from Sigma-Aldrich and used as received without further purification. Sodium hydroxide (NaOH) and toluene diisocyanate (TDI) was supplied by Aladin.

2.2 Synthesis of Ag NPs and Ag NPs/PA6.

Ag NPs/PA6 nanocomposites were prepared by two-step process including synthesis of Ag

NPs through reduction by CL and polymerization of CL. In the first step, different dosage of silver nitrate (0.0~0.85 wt%) was added to 80 g CL in the molten state. The mixture was stirred at 140 °C for 16 h under protection of nitrogen to ensure the thorough reduction of silver nitrate. In the second step, 0.8 g NaOH was added to the suspension. In order to remove trace amount of water, the mixture was vacuumed at 160 °C for 20 min. Then, 0.8 g TDI was added with stirring. Finally, the mixture was immediately poured into a mold preheated to 180 °C and polymerized in oven at 160 °C for 20 min. The as-synthesized composites were denoted as PA6-0 (Ag NPs, 0 wt %), PA6-1 (Ag NPs 0.1 wt %), PA6- 2 (Ag NPs 0.26 wt %), PA6- 3 (Ag NPs 0.5 wt %) and PA6- 4 (Ag NPs 0.85 wt %) according to the theoretical concentration of Ag NPs in the resultant composites.

2.3 Characterization.

2.3.1 UV-vis spectrum and time-of-flight mass spectrometer.

UV-vis spectroscopy was used to record the oxidized products of CL. All tests were conducted in relative to the pure CL with the same concentration. Thermal oxidation of CL initiated by oxygen were applied as comparable tests.

2.3.2 XRD.

X-ray diffraction (XRD) characterization was carried out to verify the formation Ag NPs collected from resultant mixture in the first step. PA6-0 and PA6-4 were also characterized in order to confirm Ag NPs was embedded in PA6 matrix.

2.3.3 TEM.

Transmission electronic microscopy (TEM) was carried out on a Hitachi H-800 microscope at an acceleration voltage of 120 kV. The samples were ultramicrotomed with a diamond knife on a Leica Ultracut UCT microtomed at room temperature to give nanometer thick sections.

2.3.4 Thermal analysis.

The thermal decomposition of the composites were performed over a temperature range of 50~600 °C using TA instrument SDT Q600 under nitrogen atmosphere at 10 °C/min. and by Perkin Elmer Diamond DSC instrument (Shelton, CT). The samples were heated at a rate of 20 °C/min from room temperature to 260 °C under nitrogen atmosphere and held for 5 min to remove the thermal history. And then the samples were cooled to 50 °C at the rate of 10 °C/min,

the temperature began to crystal (T_c) was recorded. The subsequent melting behavior of each sample was recorded immediately at a heating rate of 10°C/min, and the temperature at maximum melt rate was termed as melt point (T_m).

2.3.5 Viscosity average molecular weight of PA6 molecules

The viscosities of dilute polymer solutions were measured in formic acid (85 wt%) at 20 °C in a Ubbelohde viscosimeter that had a flow time of more than 100 sec for the pure solvent. The solutions contained 0.52 g of polymer per 100 ml of solvent. The results from the measurements were treated by the graphical extrapolation to zero concentration by a standard procedure.

2.3.6 FTIR.

The Broker Vector 22 FTIR spectrometer was used to investigate the structure of the as-synthesized particles and resultant composites. Spectrum was collected in attenuated total reflectance (ATR) mode with 40 scans and 2 cm⁻¹ resolution in the range of 4000–400 cm⁻¹.

2.3.7 ¹³C NMR.

PA6-0 and PA6-4 was chosen as a comparison to investigate the backbone of resultant polyamide molecules by means of ¹³C NMR. The same procedure for sample preparation was applied. For typically, 0.5 g PA6-4 nanocomposite was dissolved in 99.5 g 85 wt% formic acid. After detaching Ag NPs from solution via centrifugation. The supernatant was kept at 80 °C for 24 hours in order to evaporate formic acid. The residual solid washed another two rounds through repeating the former procedure.

NMR samples were prepared by dissolving the purified polyamide derived from PA6-0 and PA6-4 to give a sample with 5 wt% polymer in a binary solvent consisting of a 4:1 ratio of TFE to CDCl₃. Solution ¹³C NMR spectra were collected on a VNMRS 600 MHz NMR. A 5-mm NMR probe was used with an average of 8,000 scans to give sufficient signal-to-noise signals. The chemical shift was recorded with respect to TMS.

3 Results and Discussions

3.1 Synthesis of Ag NPs

Preparation of Ag/PA6 nanocomposites includes two successive steps: 1) reduction of silver nitrate by CL to synthesize Ag NPs; 2) polymerization of residual CL. A schematic diagram in Figure 1 summarizes the process of successive *in situ* synthesis of Ag/PA6 nanocomposites.

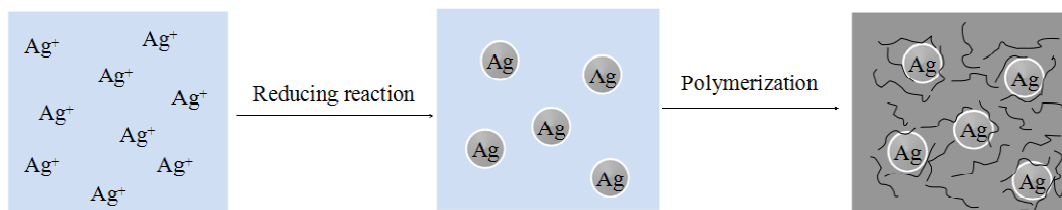


Figure 1. Schematic diagram of successive *in situ* synthesis of Ag/PA6 nanocomposite.

During the synthesis of Ag NPs, the color of silver nitrate and CL mixture changed gradually from clear and transparent at the beginning, to yellow, and then to black at the end of the reaction, suggesting thermal reduction of AgNO_3 . Previous reports of the change of graphene oxide to graphene by decomposition in molten CL was the indirect evidence for the reducibility of CL.⁷ The UV-vis spectra of pure CL treated by different reactants were recorded and the results are shown in Figure 2. Pure CL heated at 140°C for 16 hours under the protection of nitrogen shows no absorption in the range of 220–500 nm (Curve 1). On the other hand an intensive absorption at 240 nm appeared (curve 2 and curve 3) when CL was treated by oxygen (O_2 , 30 ml/min) and silver nitrate at 140°C for 16 hours. The same absorption wavelength indicates that the same product is generated. It seems that silver nitrate, playing the role of oxidizing agent as oxygen,⁸ triggers the oxidation of

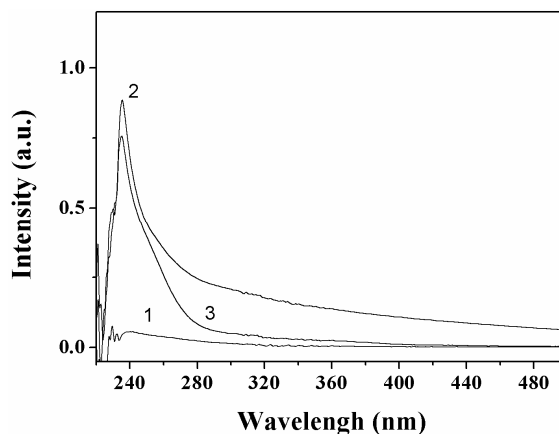


Figure 2. UV-spectrum of CL treated at different conditions. Curve 1 represents the pure CL treated under the protection of argon. Curve 2 and curve 3 illustrate the CL treated by silver nitrate and by oxygen, respectively.

CL at elevated temperature. Comparison of ^{13}C NMR spectrum of CL oxidized by O_2 and silver nitrate with respect to pure CL were recorded, and no difference (Figure 1S) was observed. Although there are several published works analyzing impurities and oxidation products of caprolactam,¹⁶ the results are confusing. That may be why little analytic information about

adipimide and adipic acid monoamide has been provided in previous studies.

The test of conductivity showed that the mixture composed of 0.17 g silver nitrate and 20 g CL was $\sim 100 \mu\text{S}\cdot\text{cm}^{-1}$ (140 °C), while the conductivity of silver nitrate aqueous solution was greater than $10^5 \mu\text{S}\cdot\text{cm}^{-1}$ at the same concentration (25 °C). This indicated that silver nitrate was partly ionized in molten CL, and the concentration of silver ions from silver nitrate in molten CL was very low. As a consequence, the low concentration of silver ions kept the reaction of silver nitrate with CL at a moderate rate. In the *in situ* preparation of NP-filled polyamide composites, CL was always used as dispersant of NPs without using other solvents.^{2c,10} As a result, potential particle aggregation of nanoparticles caused by solvent evaporation was effectively avoided. Many metal salts could be completely dissolved in molten CL, and metallic oxide NPs could be generated when a precipitator (sodium hydroxide) was added¹⁸. The nanoscale size of the as-prepared particles could be attributed to the coordination of the metal ion/atom by CL.¹¹ The typical coordinating effect between CL and Ag NPs will be illustrated in the section 3.4. Thus, combining of coordination between silver atoms and CL with the moderated rate of reduction of silver nitrate, leads to production of nanosize silver particles.

3.2 XRD pattern of Ag NPs and corresponding composites

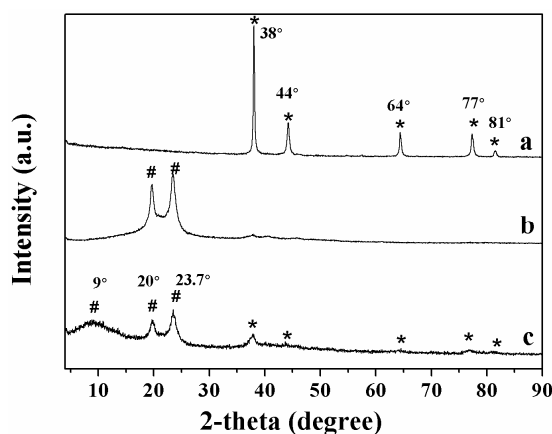


Figure 3. XRD profiles of Ag NPs and nanocomposites. **a:** Ag NPs precipitated at the end of first step (before the polymerization of CL). **b:** PA6-0. **c:** PA6-4.

Fig. 3 shows the X-ray patterns of PA6-0 and PA6-4, as well as Ag NPs precipitated from molten CL. The diffraction peaks centered at 38°, 44°, 64°, 77° and 81°, which have been shown in pattern (a), correspond to the lattice planes of (111), (200), (220), (311) and (222) facet, respectively. This is consistent with the standard XRD profile of metal silver (JCPDS-04-0783

file), which verified the formation of Ag NPs through the reduction by CL. It is well established that PA6 consists primarily of α and γ -form crystals, with the relative amounts dependent on synthesis methods and treatments. The diffraction peaks at 20° and 23.7° , are ascribed to $(200)_\alpha$ and $(002)_\alpha/(202)_\alpha$ reflections, as seen in Fig. 3(b). For the profile of PA6-4 (Fig.3c), in addition to the diffraction peaks of the α form and the typical reflections of Ag NPs, a reflection at $2\theta=9^\circ$ has arisen, corresponding to $(020)_\gamma$. It was apparent that the as-synthesized Ag NPs induced the formation of γ -form crystals in the *in situ* polymerization of CL.

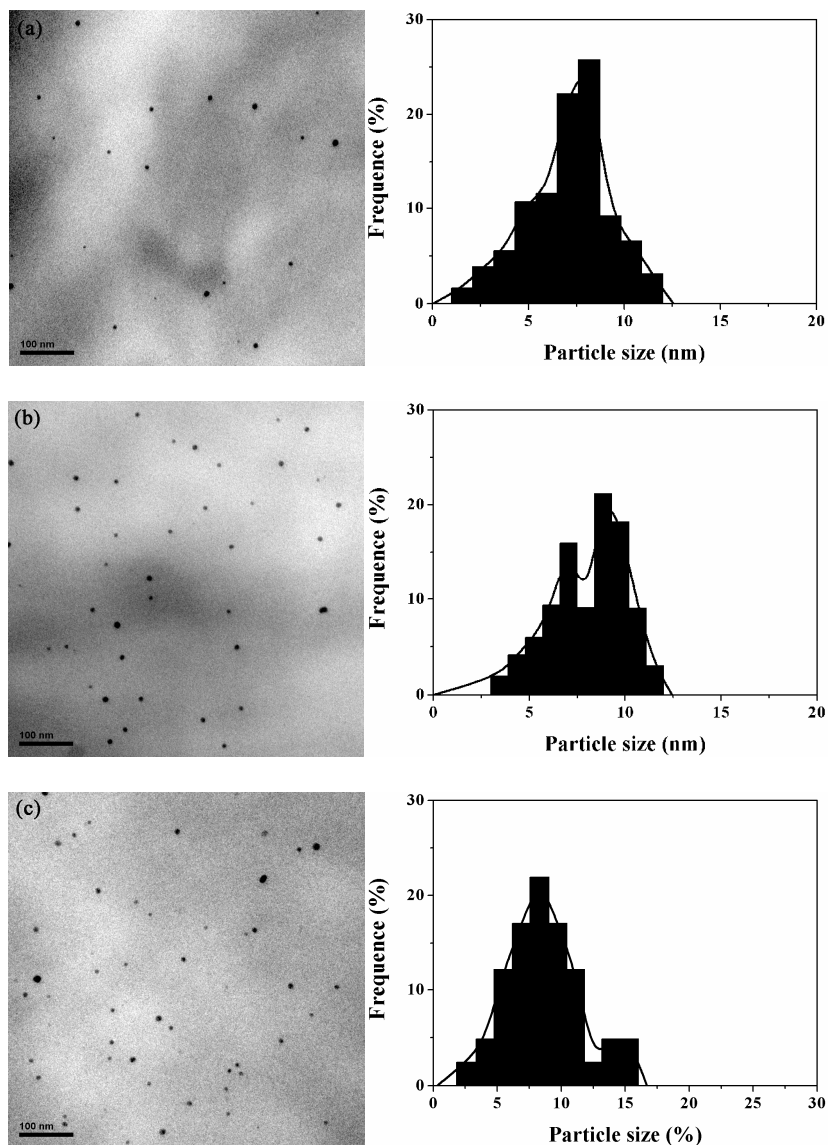
Some studies have explored the differences between PA6 nanocomposites synthesized by *in situ* polymerization and by melt processing. According to studies of Vander Hart et al.,¹² the silicate layers promoted the γ -form regardless of the formation technique. The information provided by X-ray scattering indicated that the clay platelets in these two types of nanocomposites disturbed the crystallization, and the extent of platelet-crystallite interactions was governed by the technique used to prepare the nanocomposites.^{2d} It seems that the nature of the bond between the fillers and polyamide chains influenced filler-crystallite interactions and then the crystalline morphology. And we propose that the same effect is occurring here with Ag NPs.

3.3 Morphology of Ag NPs embedded in PA6 matrix

The morphology of as-synthesized Ag NPs embedded in the polyamide matrix was recorded by TEM. The micrographics and the corresponding particle size statistics are illustrated in Figure 4. For the sample of PA6-1, the Ag NPs were smaller than 13 nm. They were distributed in the range of 6–8 nm. In the case of PA6-2, a lower shoulder located in the range of 6–8 nm and another higher shoulder corresponding to 8–12 nm co-existed in the profile. With increase of Ag NPs loading (PA6-3), some particles were as large as 15 nm. A significant decrease in the population of large particles lead to an alteration in the relative content of them with respect to that of PA6-2. With further increase of Ag NPs loading (PA6-4), the content of particles with moderate size increased. Particles larger than 17 nm emerged as well. The co-existing small particles and large ones generated a more broad size distribution.

As described above, the particles were all smaller than 25 nm and no aggregation of Ag NPs was observed. We speculate that the coordination of CL with silver ions was responsible for maintaining small particle size and preventing aggregation during particle growth. Thus the size

and size distribution of Ag NPs were controlled in this procedure. In this process, CL acts as a multifunctional reagent: reducing agent, protecting agent and solvent, all in one. This complicated the growth of silver particles in molten CL, and eventually the morphology of resultant Ag NPs. The subsequent polymerization of CL may have generated long chain polyamide and provided further protection for Ag NPs, ensuring the homogeneous distribution of Ag NPs in resultant polyamide matrix. This speculation will be discussed in the next parts.



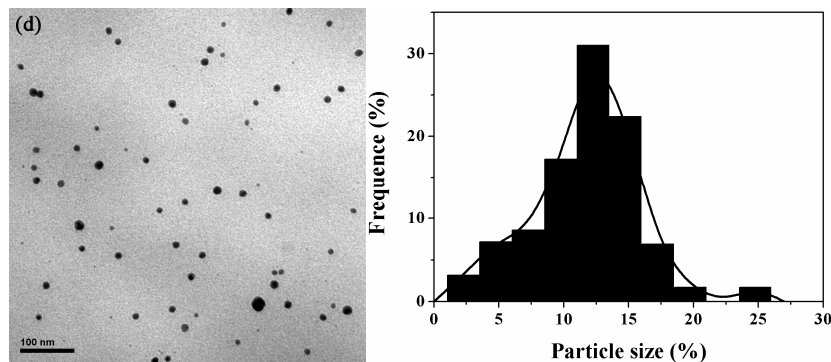


Figure. 4 Morphology of Ag NPs embedded in PA6 matrix. The labels from (a) to (d) correspond to PA6-1, PA6-2, PA6-3 and PA6-4, respectively. Because of no addition of silver nitrate, there was no Ag NPs produced, thus the graph of PA6-0 was not recorded

3.4 Protection provided by molecules of CL and PA6

In order to illustrate the protection for Ag NPs, the FTIR spectrum of Ag NPs precipitated from molten CL and polymerized CL were recorded and are shown in Figure 5. For pure CL in Figure 6(a), the absorption peaks appearing at 1660 cm^{-1} , 2932 cm^{-1} and over 3000 cm^{-1} are ascribed to stretch vibration of C=O, C-H, and N-H, respectively. The FTIR spectrum of Ag NPs-CL (AgNPs precipitated from molten CL) shared the vibration of C-H with that of CL, and a red shift was clearly observed. The signals of C=O and N-H were not detected for the Ag NPs precipitated from CL. This was probably because the CL absorbed onto the surface of Ag NPs occurred through the coordination of O and N of CL with silver. This resulted in the disappearance of the signals of the C=O and N-H bonds.¹³ In Figure 5(b), pure PA6 and AgNPs-PA6 (AgNPs precipitated from PA6-4) showed the characteristic vibrations of PA6. For example, stretch vibrations of N-H, C-H and C=O were inherited by Ag NPs-PA6. The intensity ratios $I_{\text{N-H}}/I_{\text{C-H}}$ and $I_{\text{C=O}}/I_{\text{C-H}}$ of Ag NPs-PA6 were lower than those of pure PA6, and a red shift for all three peaks was presented in the spectra. Contrary to Ag NPs-CL, Ag NPs-PA6 showed intense resonance of N-H and C=O. This indicated that not all of the N and O in PA6 molecules coordinated with silver. It means that part of PA6 molecules stretched out of the absorption layer, providing sterical protection. And then uniform distribution of Ag NPs in PA6 matrix could be expected as showed in Figure 5. The analysis of Figure 5(a) and Figure 5(b) indicated that the protection provided by CL was continued by the molecules of PA6 after the polymerization of CL. This was clarified in the combined FTIR spectrum of Ag NPs-CL and Ag NPs-PA6 as shown in Figure 5(c).

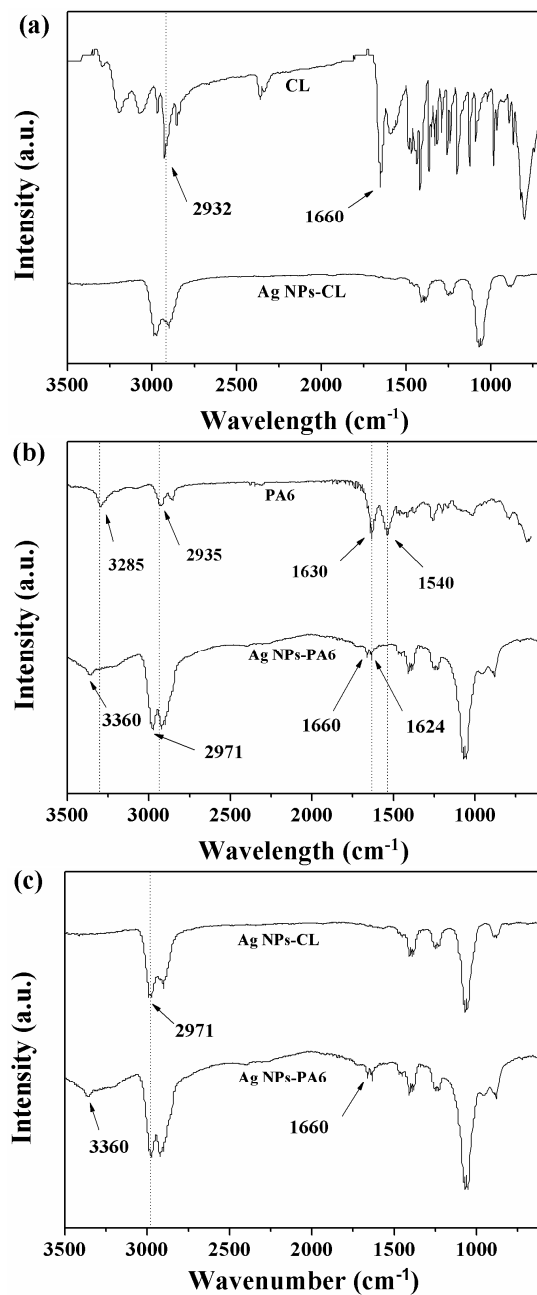


Figure 5. FTIR spectrum of Ag NPs. Ag NPs-CL and Ag NPs-PA6 designated Ag NPs precipitated from molten CL before polymerization and Ag NPs separated from nanocomposite PA6-4. Pure CL and PA6 prepared using no addition of silver nitrate were devoted as references.

3.5 Structure of PA6 molecules and nanocomposites

The FTIR spectrum was used to illustrate the effects of *pre in situ* synthesized procedure on the molecular structure of PA6. For comparison, the spectra of PA6-0 (no Ag NPs) and PA6-4 (maximum Ag NPs loading) were recorded, (Figure 6). In the spectrum of PA6-0 (Fig 6(a)), the peak at 3285 cm⁻¹ corresponded to stretching vibrations of N-H.¹⁴ The peaks located at 2935 and

2875 cm^{-1} are assigned to the asymmetric and symmetric stretching vibration of CH_2 . The absorption at 1630 and 1540 cm^{-1} was attributed to amide I and amide II mode, respectively.¹⁵ The absorption region of 1466–1250 cm^{-1} can be assigned to other vibrations modes of CH_2 and amide III, while the peaks presented in fingerprint region arose from the CO-NH in-plane vibration and amide V mode. The peaks in this range are mixed and are complicated by the contributions from crystal and amorphous phase.

The PA6-4, consisting of 0.85wt% Ag NPs shares a similar spectrum with that of PA6-0, except for the change in the relative absorption for amide I and amide II mode. Amide I mode can be considered to be comprised of contributions from the C=O stretching, the C-N stretching, and the C-C-N deformation vibrations.¹⁰ The amide II band is a mixed mode containing contributions from the N-H in-plane bending, the C-N stretching, and the C-C stretching vibrations.¹⁰ Normal coordinate calculations revealed that the potential energy distribution of amide I is comprised of 77 % C=O stretch and 14 % C-N stretch, while that of amide II comprised 43 % N-H in-plane bend and 26 % C-N stretch.²² Both amide I and amide II mode are conformationally sensitive modes and have been widely used to investigate the chemical changes in PA6 and its nanocomposites. The Ag NPs embedded in PA6-4 matrix may bind to the polar atoms, such as N and O, in the PA6 molecule, and then distort the energy distribution of amide I and amide II. The change in the relative intensity of amide I and amide II modes is consistent with this interpretation.

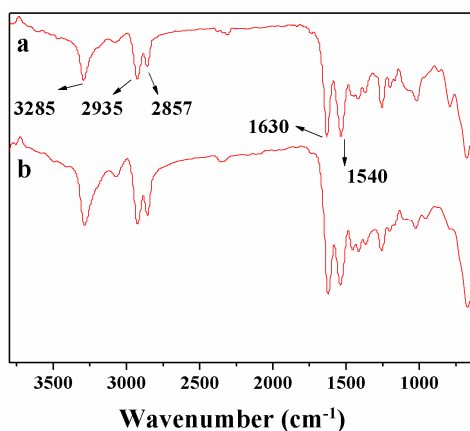


Figure 6. FTIR spectrum of Ag/PA6 nanocomposites. a and b correspond to PA6-0 and PA6-4, respectively.

Subsequent study of the structure of the PA6 matrix was carried out by ¹³C NMR. Spectra of PA6-0 and matrix of PA6-4 were recorded. Figure 7 illustrates the peak position labeling

employed. For the sample of PA6-0, signals from downfield to upfield are assigned to the carbon backbone of PA6-0, corresponding to C₆ (178.7 ppm), C₁ (41.9 ppm), C₅ (38.5 ppm), C₂ (30.7 ppm), C₃ (28.4 ppm), C₄ (27.6 ppm), respectively. It was apparent that the peaks for PA6-4 and PA6-0 are identical. This confirms the similarity in chemical structure of the two matrices.^{12, 16} It seems that the *pre in situ* procedure involving synthesis of Ag NPs did not induce variance in backbone of the resulting polymerized PA6.

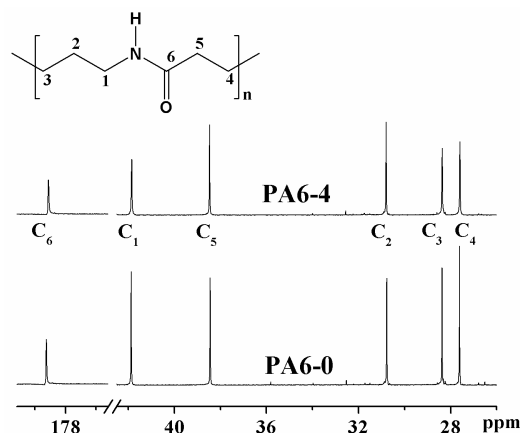


Figure 7. C¹³-NMR spectra of matrix of PA6-0 and PA6-4.

3.6 Thermal behavior of as-synthesized nanocomposites

The polymers showed in general the characteristics of those that had been obtained by polymerizing CL pre-treated with silver nitrate. Increasing the extent of oxidation of the CL results in a decrease in the molecular weight of the corresponding PA 6 as shown in Table 1. This agrees well with the results disclosed by H. K. Reiriischuessel that the molecular weight depends considerably upon the extent to which the corresponding lactam has been exposed to oxygen.^{8b} In addition to the increasing consumption of CL resulting from the increased dosage of silver nitrate in the synthesis of Ag NPs, the decomposition of caprolactam hydroperoxide yields additional compounds that may interact with the growing polymer chain. Therefore, a decrease in molecular weight could be expected.

Thermoanalysis is a powerful and convenient way to detect the effects of NPs on the molecular movement, which can be reflected by the heat flow corresponding to different morphologies of nanocomposites. The cooling and heating scan of DSC of as-synthesized PA6 and its composites with Ag NPs are shown in Figure 8. The information about onset and maximum crystallization temperature ($T_{c-onset}$ and T_{c-max}), melt point (T_m), as well as level of crystallinity (X_c)

are summarized in Table 1.

The $T_{c-onset}$ gradually decreased from 191.1°C for pure PA6 to 190.4 °C for PA6-1 that incorporated 0.1wt% Ag NPs. This indicated that the pre-synthesized Ag NPs slightly retarded the nucleation of PA6 matrix. This trend was enhanced by increasing Ag NPs loading. Decrease of $T_{c-onset}$ elucidated that *in situ* synthesized Ag NPs retard the growth process, agreeing well with the increase of time of half-crystallization ($t_{1/2}$). The gradual increased population of Ag NPs should be responsible for this result. Actually, NPs are inclined to serve as a heterogeneous nucleating agent at low concentration, the distance between dispersed particles is large so it is relatively easy for the nucleation sites to incorporate surrounding polymer, which would lead to a fast crystallization. However, at high concentrations of NPs, diffusion of polymer chains to the growing crystallite is hindered. Thus, a retardation effect on crystallization can be expected at high concentration of NPs.¹⁷ In our system, the strong coordination between Ag NPs and polyamide seemed to mask the heterogeneous nucleating effect in all the concentrations, and eventually retard crystallization.

In general, adding Ag NPs resulted in a reduction in T_{c-max} , $X_{(c)}$ and T_m . The level of reduction was different from sample to sample for these three characteristics. The differences can be attributed to the alteration of the molecular weight of polyamide, the size and size distribution of pre-synthesized Ag NPs and concentration of them, as well as the coordination effects between Ag NPs and polyamide chains. Combination of these factors is expected to produce a complicated mode for the mobility of polyamide chain, and thus to disturb the stacking of polyamide chain in crystal, eventually leading to reduction in T_{c-max} , $X_{(c)}$ and T_m .

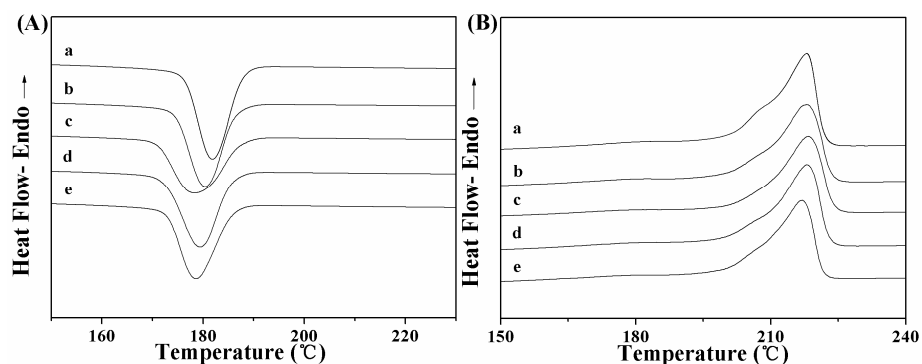


Figure 8. DSC cooling and heating scan thermograms of as-synthesized PA6 and Ag/PA6 nanocomposites with different silver loading. The curves from (a) to (e) correspond to sample of PA6-0, PA6-1, PA6-2, PA6-3 and PA6-4, respectively.

Table 1. Properties of resultant Ag/PA6 nanocomposites

Samples	Ag NPs / wt%	$M_v / (\times 10^{-3})$	$T_{c-onset} / ^\circ\text{C}$	$T_{c-max} / ^\circ\text{C}$	$t_{1/2} / \text{min}$	$X_{(c)}$	$T_m / ^\circ\text{C}$	$T_d / ^\circ\text{C}$
PA6-0	0.00	12.4	191.1	181.8	6.89	28.6	218.1	303.9
PA6-1	0.10	11.8	190.4	180.4	7.05	26.5	218.0	304.0
PA6-2	0.26	11.4	189.8	178.3	7.18	26.6	218.1	303.1
PA6-3	0.50	10.8	189.1	179.4	7.18	27.3	217.9	301.8
PA6-4	0.85	9.6	188.6	178.5	7.20	26.9	216.7	294.9

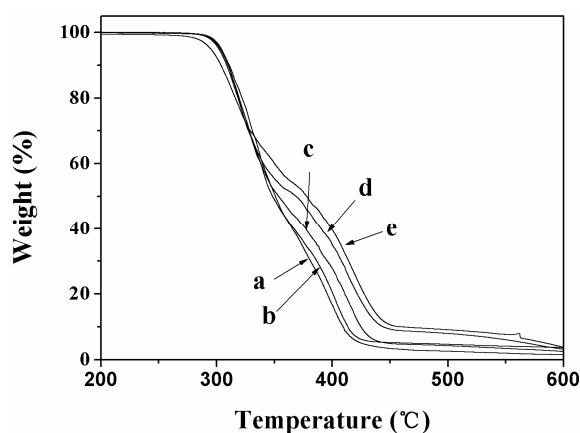


Figure 9. TGA curve of Ag/PA6 nanocomposites with different dosage of Ag NPs. The curves from (a) to (e) correspond to sample of PA6-0, PA6-1, PA6-2, PA6-3 and PA6-4, respectively.

The TGA curves of Ag/PA6 nanocomposites with different incorporation of Ag NPs were plotted in Figure 9. It can be seen that all of the composites have two-step decomposition similar to that of pure PA6. In the first step of decomposition, the 5% weight loss temperature summarized in Table 1 shows that the successive *in situ* synthesized composites generally had a lower thermal stability with an increase of Ag NPs loading. In the second step, PA6 composites decomposed at lower temperature with the increasing content of Ag NPs. In addition, a retardation effect in the second step was observed in the presence of Ag NPs and this effect gradually became more apparent with the increase in content of Ag NPs. The presence of Ag NPs with different size and size distribution, combining with variability in molecular weight, complicated the decomposition behavior, an aspect which needs more investigation.

4 Conclusions

Ag/PA6 nanocomposites were prepared by reaction of CL with silver nitrate followed by polymerization of CL. CL played the role of reducing agent and protecting agent in the *in situ* generation of Ag NPs, as well as the precursor monomer of polyamide matrix. The formation of

Ag NPs was verified by the XRD spectrum. TEM showed that the sizes of the resultant Ag NPs were less than 20 nm, and that they were uniformly distributed in the matrix of PA6. Incorporation of Ag NPs induced the formation of γ -form crystals. The molecular weight of the PA6 matrix decreased with the increase of dosage of silver nitrate because of the increasing consumption of CL by oxidation. FTIR and NMR indicated that the redox reaction of silver nitrate with CL did not influence the polyamide molecular structure. The variation in particle size and size distribution of Ag NPs complicated the thermal behaviors of the resultant nanocomposites.

Notes and references

Author information

- ^a Department of Polymer Science and Engineering, Zhejiang University, 38 Zheda Road, Hangzhou 310027, People's Republic of China.
- ^b School of Chemical Engineering, Hefei University of Technology, 193 Tunxi Road, Hefei 230009, People's Republic of China.
- ^c Shanghai Genius Advanced Materials Co. Ltd., Shanghai, 201109, People's Republic of China.

References

- (a) A. C. Balazs, T. Emrick and T. P. Russell, *Science*, 2006, **314**, 1107. (b) Z. Zhang, J.-L. Yang and K. Friedrich, *Polymer*, 2004, **45**, 3481.
- A. J. Bur, Y.-H. Lee, S. C. Roth, et al., *Polymer*, 2005, **46**, 10908; H. Xia, 2013, 60; Y. Liu and G. Yang, *Thermochimica Acta*, 2010, **500**, 13. (b) Y. Liu, T. Xie and G. Yang, *Journal of Materials Science*, 2011, **46**, 5050; (c) H. Xia, X. Zhao and G. Yang, *Materials Letters*, 2013. (d) Y. Liu, Z. Chen and G. Yang, *Journal of Materials Science*, 2011, **46**, 882. (e) T. D. Fornes and D. R. Paul, *Polymer*, 2003, **44**, 3945. (f) R. Sengupta, A. Bandyopadhyay, S. Sabharwal, et al., *Polymer*, 2005, **46**, 3343. (g) J. W. Cho and D. R. Paul, *Polymer*, 2001, **42**, 1083.
- L. Liu, Z. Qi and X. Zhu, *Journal of Applied Polymer Science*, 1999, **71**, 1133.
- X. Liu and Q. Wu, *European Polymer Journal*, 2002, **38**, 1383.
- X. Zhang, X. Fan, H. Li, et al., *Journal of Materials Chemistry*, 2012, **22**, 24081.
- H. Fong, W. D. Liu, C. S. Wang, et al., *Polymer*, 2002, **43**, 775.
- Z. Xu and C. Gao, *Macromolecules*, 2010, **43**, 6716.
- (a) B. Lánská and J. Šebenda, *Die Angewandte Makromolekulare Chemie*, 1988, **164**, 181; (b) B. Lánská, L. M. Postnikov, A. L. Aleksandrov, et al., *Collection of Czechoslovak Chemical Communications*, 1981, **46**, 2650; (c) A. Rieche and W. Schon, *Chemische Berichte*, 1966, **99**, 3238. (d) G. Dege and H. Reimschuessel, *Journal of Polymer Science: Polymer Chemistry Edition*, 1973, **11**, 873.
- (a) G. Eppert, G. Liebscher and C. Stief, *Journal of Chromatography A*, 1990, **508**, 149; (b) W. Czerwiński, M. Wiejcka, H. Malikowska, et al., *Journal of Chromatography A*, 1981, **208**, 27; (c) L. P. Friz, G. Bertuzzi and E. Bovetti, *Journal of Chromatography A*, 1969, **39**, 253.

10. T.-M. Wu and C.-S. Liao, *Macromolecular Chemistry and Physics*, 2000, **201**, 2820.
11. H. Xia and G. Yang, *Journal of Materials Chemistry*, 2012, **22**, 18664.
12. (a) D. VanderHart, A. Asano and J. Gilman, *Chemistry of Materials*, 2001, **13**, 3796; (b) D. VanderHart, A. Asano and J. Gilman, *Chemistry of Materials*, 2001, **13**, 3781.
13. A. Regiel, S. Irusta, A. Kyzioł, et al., *Nanotechnology*, 2013, **24**, 015101.
14. V. Deimede, K. Fragou, E. Koulouri, et al., *Polymer*, 2000, **41**, 9095.
15. (a) W. H. Moore and S. Krimm, *Biopolymers*, 1976, **15**, 2465. (b) D. J. Skrovanek, S. E. Howe, P. C. Painter, et al., *Macromolecules*, 1985, **18**, 1676.
16. (a) S. J. Steadman and L. J. Mathias, *Polymer*, 1997, **38**, 5297; (b) H. R. Kricheldorf and W. E. Hull, *Journal of Polymer Science: Polymer Chemistry Edition*, 1978, **16**, 2253; (c) R. D. Davis, S. J. Steadman, W. L. Jarrett, et al., *Macromolecules*, 2000, **33**, 7088; (d) R. D. Davis, W. L. Jarrett and L. J. Mathias, *Polymer*, 2001, **42**, 2621.
17. J. Ma, S. Zhang, Z. Qi, et al., *Journal of applied polymer science*, 2002, **83**, 1978.